Chapter 50
PERSIANN-CDR for Hydrology and Hydro-climatic Applications

Phu Nguyen, Hamed Ashouri, Mohammed Ombadi, Negin Hayatbini, Kuo-Lin Hsu, and Soroosh Sorooshian

Abstract Satellite-retrieved precipitation datasets represent a promising input data source to be utilized in hydroclimatic and hydrologic applications. Due to their characteristics of high spatiotemporal resolution, near real-time availability and quasi global coverage, satellite-retrieved precipitation datasets promise to provide a remedy for the long-standing issues associated with ground rainfall information. In this article, we shed light on the Precipitation Estimation from Remotely Sensed Information using Artificial Neural Networks – Climate Data Records (PERSIANN-CDR) dataset and its use in hydroclimatic and hydrologic applications. In particular, we highlight the use of PERSIANN-CDR for rainfall trend analysis, observation of extreme rainfall events such as Hurricanes, and evaluation of climate models' simulations of precipitation based on their historical performance. Regarding the use of PERSIANN-CDR for hydrologic applications, we show examples of utilizing the dataset in rainfall-runoff modeling as well as its use in rainfall frequency analysis and the development of intensity-duration-frequency (IDF) curves.

Keywords Precipitation · Rainfall · PERSIANN-CDR · PERSIANN-CCS · TMPA · CMORPH · GPCP · Hydrology · Hydroclimatology · Neural networks · Rain gauges · Brightness temperature · Mann-Kendall test · ETCCDI · CCI · JCOMM · CLIVAR · Extreme value theory · CMIP5 · IDF curves

50.1 Introduction

Precipitation is a vital component of water and energy cycle and is one of the most, if not the most, important meteorological input for hydrometeorological and climatic models (Sorooshian et al. 2011). Reliable long-term precipitation data on a global scale is essential for a wide range of hydrological, hydrometeorological, and

P. Nguyen (✉) · H. Ashouri · M. Ombadi · N. Hayatbini · K.-L. Hsu · S. Sorooshian
Center for Hydrometeorology & Remote Sensing (CHRS), University of California, Irvine, CA, USA
e-mail: ndphu@uci.edu

V. Levizzani et al. (eds.), *Satellite Precipitation Measurement*, Advances in Global Change Research 69, https://doi.org/10.1007/978-3-030-35798-6_26

climatological applications. Gauge-based data sets generally provide long-term, direct physical measurement of precipitation, however, their sparse point measurements as well as susceptibility to certain errors have elevated the importance of satellite-based rainfall estimates (Kidd et al. 2017; Rana et al. 2015; Xie and Arkin 1997).

Satellite observations make up for such deficiencies by providing coverage that is spatially more homogeneous and temporally complete globally (Kidd and Levizzani 2011; Xie et al. 2003). Over the past recent decades, the availability of satellite-based observations has motivated researchers to investigate several hydroclimatic processes and develop methods for the incorporation of these datasets in hydrologic applications. Sun et al. (2018) provided a summary of major satellite-related precipitation data sets that are currently available and Maggioni et al. (2016) presented a consolidated and detailed review of the algorithms used in satellite precipitation data sets. Some of the currently operationally available satellite-derived data sets are the Tropical Rainfall Measuring Mission (TRMM) Multisatellite Precipitation Analysis (TMPA) (Huffman et al. 2007), the Precipitation Estimation from Remotely Sensed Information using Artificial Neural Networks – Climate Data Records (PERSIANN-CDR) (Ashouri et al. 2015), and the Climate Prediction Center (CPC) morphing technique (CMORPH) (Joyce et al. 2004) products.

The focus of this chapter is on the applications of PERSIANN algorithms family, particularly PERSIANN Climate Data Record (PERSIANN-CDR, Ashouri et al. 2015). This algorithm provides long-term, high-resolution, satellite-based precipitation estimates for hydroclimatological applications. PERSIANN-CDR's daily (sub-daily; 3-hourly) and 0.25° precipitation data from 1983 to present makes it suitable to study the behavior of extreme precipitation patterns on a global scale over the past three decades (Hsu et al. 1997; Sorooshian et al. 2000). This satellite-based precipitation product provides daily precipitation estimates from the year 1983 to present at a resolution of 0.25° on the archive of Gridded Satellite (GridSat-B1) IR satellite data (Ashouri et al. 2015; Lee 2014). PERSIANN-CDR utilizes an artificial neural network to assign a surface rain rate based on brightness temperature retrievals of infrared information from geostationary Earth-Orbiting (GEO) satellites, specifically from the archive of Gridded Satellite (GridSat-B1). The artificial neural network is trained with stage IV hourly precipitation data from the National Centers for Environmental Prediction (NCEP). The high-resolution PERSIANN estimates are then adjusted by the GPCP (Global Precipitation Climatology Project) data at a resolution of 2.5° to downscale and remove the bias from the precipitation estimates (Ashouri et al. 2015). Toward this aim, the merged analysis (1979-present) from monthly GPCP global precipitation products is utilized for each month of the 30-year period at each 2.5° grid box of PERSIANN data. The corresponding 0.25° 3-hourly PERSIANN rain-rate estimates are aggregated to monthly scale after applying a proper threshold value to filter out pixels associated with no rain-rate. Then a correction factor based on the ratio of 2.5° monthly GPCP precipitation and PERSIANN rain-rate estimates at each 0.25° pixel is calculated and adjusted to be applied to 3-hourly PERSIANN estimate. GPCP version 2.2 (http://precip.gsfc.nasa.gov, last accessed 24 Nov. 2018), and GPCP 1° daily precipitation product

(Huffman et al. 2001) are used for correction and evaluation purposes respectively. For more detail regarding the process of adjusting PERSIANN data using monthly GPCP data refer to Ashouri et al. (2015).

The resulting final PERSIANN-CDR data is available through NOAA NCEI CDR program at https://www.ncdc.noaa.gov/cdr/atmospheric/precipitation-persiann-cdr (last accessed 24 Nov. 2018). PERSIANN-CDR has been widely used and validated by the scientific and user communities (Miao et al. 2015; Yang et al. 2016; Tan et al. 2015; Zhu et al. 2016; Duan et al. 2016, among many others). The availability of historical record (+35 years) at high spatiotemporal resolution of satellite-based data have enabled the investigation of trends and changes of many hydroclimatic processes. For example, the PERSIANN-CDR dataset has been used in investigating the response of precipitation regimes to the Amazonian deforestation (Khanna et al. 2017). An additional example is examining the increased frequency and intensity of floods in the Niger River basin during the last decade (Casse and Gosset 2015). The global PERSIANN Cloud Classification System (PERSIANN-CCS) is another member of the PERSIANN family of rainfall retrieval algorithms. It has a higher spatio-temporal resolution (0.04° and 30 min) compared to PERSIANN-CDR. It is derived from IR brightness temperature data from GEO satellites and uses PMW measurements from LEO satellites to update its parameters. This patch-based cloud classification and rainfall estimation algorithm uses histogram matching and exponential regression to fit curves to the plots of pixel brightness temperature versus rainfall rate (Hong et al. 2007).

The use of satellite-retrieved precipitation is promising mainly due to its characteristics of real-time information, near-global coverage and high spatiotemporal resolution.

Real-time (or near real-time) information provided by satellite-based precipitation proved to be invaluable in monitoring and capturing the development of cyclones since it has the ability of providing rainfall intensity information over the oceans before cyclones make landfall. In addition, it consistently provides rainfall estimates over land during such events without being affected by the high-speed wind and torrential rainfall. An example of real-time monitoring of cyclones using satellite-based precipitation is the tracking of Typhoon Haiyan (Nguyen et al. 2014) which struck Southeast Asia in the year 2013. In the study of Nguyen et al. (2014), PERSIANN-CCS dataset has been used in monitoring the overall propagation and estimating rainfall intensities during the event.

Overall, PERSIANN datasets have been used in a wide range of studies during the last decades; these studies can be classified in three categories. Firstly, hydrometeorological studies such as investigating diurnal rainfall patterns (Sorooshian et al. 2002), drought monitoring (Zambrano et al. 2017) and evaluating climate model simulations of precipitation (Nguyen et al. 2018). Secondly, hydrologic applications such as examining the use of satellite-based precipitation in runoff prediction (e.g., Behrangi et al. 2011; Ashouri et al. 2016a; Liu et al. 2017; Hsu et al. 2013) and use of satellite-based precipitation in rainfall frequency analysis (e.g., Gado et al. 2017; Ombadi et al. 2018). Finally, these datasets have been integrated with other precipitation estimates from different sources including

gauge, radar and satellite to compile comprehensive precipitation datasets (e.g., Chiang et al. 2007). In the subsequent sections of this chapter, some of these applications will be discussed in more detail.

50.2 Hydro-climatic Applications

50.2.1 RainSphere for Global Precipitation Analysis and Visualization

CHRS RainSphere is one of the applications derived from PERSIANN-CDR (Ashouri et al. 2015) precipitation estimates records to facilitate trend analysis in annual global precipitation and future precipitation projections studies. CHRS RainSphere interface includes search capabilities as well as the ability to automatically generate reports with basic statistics and summaries. It has several options for visualization of precipitation data along with additional spatial reference so users can quickly and easily extract meaningful information. (Nguyen et al. 2017a, 2018).

Figure 50.1 shows the map visualization for the accumulated total precipitation for 1 January to 31 December 2014 along with options to explore spatial patterns of

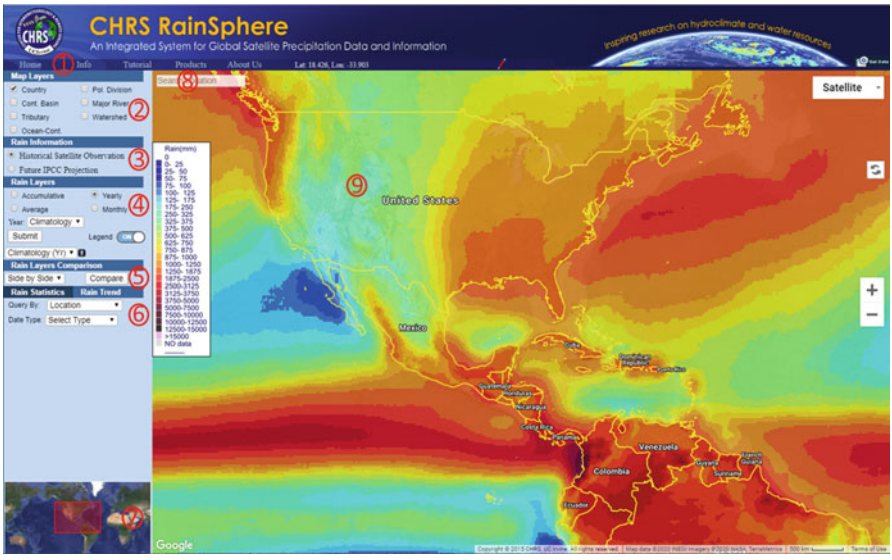

Fig. 50.1 CHRS RainSphere interface: (1) Navigation Bar, (2) Map Layers, (3) Rain Information, (4) Rain Layers, (5) Rain Comparison, (6) Rain Statistics, (7) Reference Map, (8) Search Location, (9) Map Canvas (URL: http://rainsphere.eng.uci.edu/, last accessed 24 Nov. 2018). (Nguyen et al. 2017a, 2018)

precipitation within a specified area. In this case the "Country" map layer is added for spatial reference, and additional options for spatial reference include political divisions (e.g., states and provinces), continental basins, major rivers, tributaries, and watersheds. Other than rain information and map layers, rain comparison, and rain statistics are further information that users are able to extract based on their requirements.

CHRS RainSphere also provides users with the general trends and average behavior for the selected area during the selected time span using a bar plot with precipitation amount in mm for each time step (day, month, or year). Corresponding mean and linear regression along with the Mann-Kendall test (Mann 1945; Kendall 1976) results automatically will be generated and reported as part of the statistics suite.

The Mann-Kendall test is used to statistically investigate whether to reject the null hypothesis of no trend in the data, with a p value equal to or greater than 0.05 in this calculation indicating acceptance of the null hypothesis. Below that value the alternative hypothesis is accepted with a smaller value of p indicating higher confidence that a trend exists. This test has been demonstrated as a useful tool for evaluating global climate trends (Damberg and AghaKouchak 2014). For illustration, Fig. 50.2 displays the statistical summary for yearly precipitation in the state of California from 1983 to 2015.

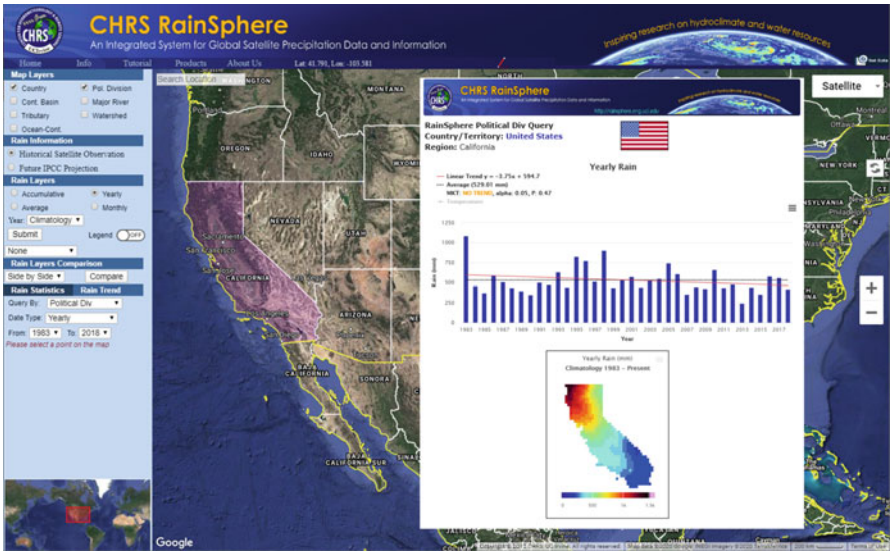

Fig. 50.2 Downloadable Rain Query Report including: Rain Linear Trend, Rain Average, Mann-Kendall Test. [http://rainsphere.eng.uci.edu/, last accessed 24 Nov. 2018]

50.2.2 Evaluation of PERSIANN-CDR on Extreme Events

One of the main applications of PERSIANN-CDR's long-term precipitation climate data record is studying extreme precipitation events. As an example, we looked at Hurricane Katrina, one of the five deadliest and the costliest hurricanes ever to strike the US Katrina hit Southeast US in August 2005 and caused inflicted loss of lives and economic damages in the region (Graumann and National Climatic Data Center 2006). As shown in Fig. 50.3, PERSIANN-CDR (a) shows similar precipitation patterns to the radar data (b). Moreover, unlike Stage IV radar data which suffers from blockages in mountainous regions or outages during a catastrophic event, the spatial coverage provided by PERSIANN-CDR is very valuable and captures a wide view of the precipitation and hurricane landfall. In order to investigate the performance of PERSIANN-CDR compared to other high-resolution satellite-based precipitation products, the TMPA V7 research version product is used. PERSIANN-CDR and TMPA were each compared to Stage IV radar data. As shown in the scatterplots in Fig. 50.3, PERSIANN-CDR shows a higher correlation coefficient than TMPA however, the bias in TMPA is lower than that in PERSIANN-CDR. It is noteworthy that the TMPA research version is also bias corrected with GPCP data at monthly scale. The differences observed between TMPA and PERSIANN-CDR performance mainly relate to 1) the difference in the algorithm of these two products, and 2) the inputs to these algorithms. During validation and performance comparison, it is imperative to note that, gauge-information aside, PERSIANN-CDR only uses IR data as its input whereas TMPA uses, passive microwave, IR, and radar data.

Expert Team on Climate Change Detection and Indices (ETCCDI) (Klein Tank et al. 2009), sponsored jointly by the World Meteorological Organization (WMO)

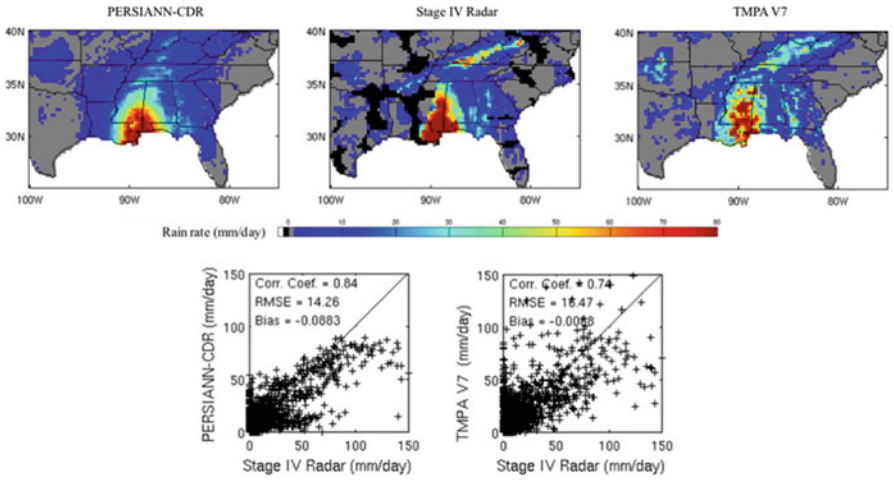

Fig. 50.3 Rainfall (mm day^{-1}) over land during Hurricane Katrina on 29 August 2005 from: (**a**) PERSIANN-CDR, (**b**) Stage IV Radar (Lin and Mitchell 2005), and (**c**) TMPA v7 (Huffman et al. 2007). Black and gray pixels show radar blockages and zero precipitation, respectively. (Adapted from Ashouri et al. 2015)

Commission for Climatology (CCl), the Joint Commission for Oceanography and Marine Meteorology (JCOMM), and the World Climate Research Program (WCRP) on Climate Variability and Predictability (CLIVAR), has defined various precipitation indices for studying extremes. Using two count related indices, the annual average count of days when rainfall $\geq$10 mm (R10mm), and the annual average count of days when rainfall $\geq$20 mm (R20mm), the performance of PERSIANN-CDR in reproducing the number of rainy days over the US for 1983–2011 is investigated against the 0.25° daily CPC Unified Gauge-Based Analysis of Precipitation data (Xie et al. 2010). As shown in Fig. 50.4, in general PERSIANN-CDR reproduces the same patterns as depicted in CPC. PERSIANN-CDR, however, underestimates R10mm and R20mm on the west cost of the US. The underestimation over the Sierra Nevada Mountains might be most likely due to 1) the type of precipitation in this region, being snow dominated rather than rain and/or 2) being orographic rain which satellite and radar have difficulties to fully capture.

The scatterplots and the statistics, Correlation Coefficient (Corr. Coef.), Root Mean Square Error (RMSE), and Bias of PERSIANN-CDR against CPC are shown in Fig. 50.5. As shown, correlation coefficient is high in both cases (> 0.9). PERSIANN-CDR tends to show a lower bias in R10mm than R20mm. Over mountainous regions like Sierra Nevada mountains, the agreement between PERSIANN-CDR and CPC degrade.

In another extreme precipitation study the performance of PERSIANN-CDR in capturing extreme rainfall events was validated against gauge observation in China. East Asia (EA, Xie et al. 2007) ground-based gridded daily precipitation data set is comprised of more than 1300 ground-based stations across China interpolated into 0.5° × 0.5° grid boxes using the Optimal Interpolation (OI) method.

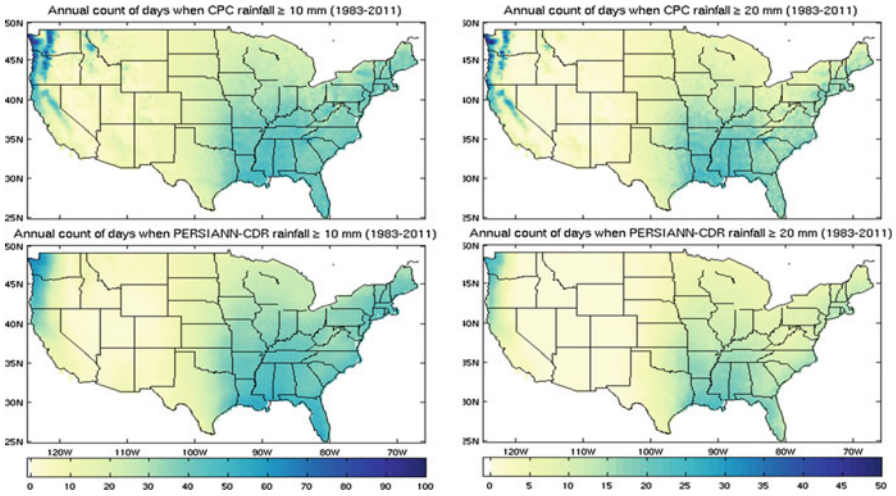

Fig. 50.4 Annual average count of days where rainfall $\geq$10 mm (left column) and rainfall $\geq$20 mm (right column) for CPC (top), and PERSIANN-CDR (bottom) for 1983–2011

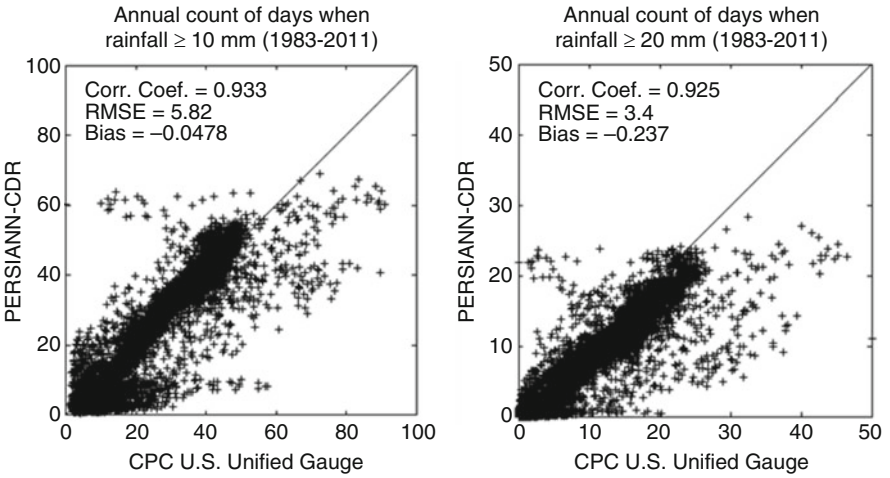

Fig. 50.5 Scatter plots of the annual average count of days where rainfall ≥10 mm (left column) and rainfall ≥20 mm (right) for PERSIANN-CDR against CPC. Correlation coefficient, RMSE, and Bias are shown on the plots

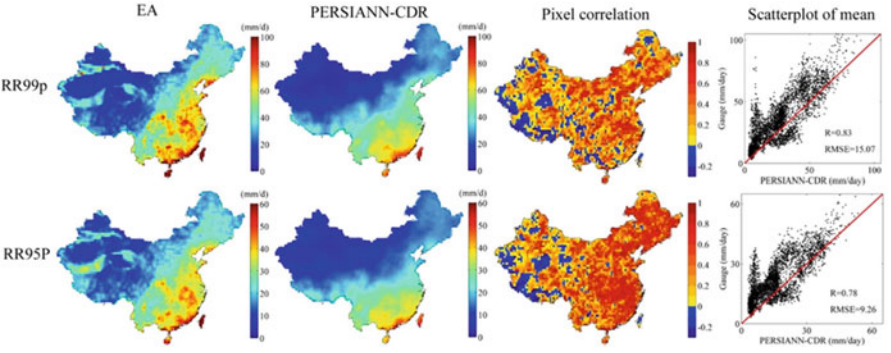

Fig. 50.6 The 99th and 95th percentile indices of extreme daily precipitation from the EA data set (first column), and PERSIANN-CDR (second column). The spatial correlation distribution and the scatterplots of the indices from the EA and PERSIANN-CDR data sets are shown in the third and fourth columns, respectively. The stippled areas in the third column show the significant correlation coefficient at the 95% level (Miao et al. 2015)

Figure 50.6 illustrates the performances of PERSIANN-CDR in capturing the 99th (RR99p) and 95th (RR95p) percentile indices of the daily precipitation during the period of 1983–2006. As shown, PERSIANN-CDR captures the spatial distribution of RR99p and RR95p similar to what the EA data set shows, with increasing RR99p and RR95p from North to South and from East to West. In addition, the scatterplots show high correlation coefficient between the percentile indices extracted from PERSIANN-CDR and EA datasets (Miao et al. 2015, for a complete analysis on all extreme precipitation indices). It is noteworthy the agreement

between PERSIANN-CDR and EA dataset was closer in data rich regions in the west and south. As shown in Fig. 50.6, correlation coefficients in dry and arid regions in the western (Tibetan Plateau) and northwestern (Taklamakan Desert) China are relatively low. The main reason for this discrepancy is lack of enough gauge stations in these regions. With lesser and much sparse gauge stations in this region, the error and uncertainty that is introduced in the interpolated EA product could be significant.

In order to consider the effects of climate change, Ashouri et al. (2016a, b) developed non-stationary statistical models based on Extreme Value Theory (EVT) to investigating whether changes in our climate system have altered the probability distribution of climate extremes. The study – carried out over US – could identify regions where over the past three decades, the odds of record-setting extreme precipitation events have increased.

50.2.3 Evaluation of CMIP5 Model Precipitation

General circulation models (GCMs) are important tools for simulating the current state of the climate and projecting future changes of precipitation under different greenhouse gas emission scenarios. The predictive skills in precipitation simulations of the Coupled Model Intercomparison Project Phase 5 (CMIP5) models (Taylor et al. 2012), especially in capturing extreme precipitation events, are highly model dependent. PERSIANN-CDR was used as a tool to evaluate the ability of 32 CMIP5 models to capture the behavior of extreme precipitation estimates globally (Nguyen et al. 2017b). The work uniquely defines study regions by partitioning global land areas into 26 groups based on continent and climate zone type then uses PERSIANN-CDR as a baseline to investigate 8 extreme precipitation indices: (a) Total: R99pTOT – annual total precipitation when daily precipitation amount on a wet day >99 percentile, R95pTOT – annual total precipitation when daily precipitation amount on a wet day >95 percentile, R10mmTOT – annual total precipitation when daily precipitation amount $\geq$ 10 mm, and PRCPTOT – annual total precipitation in wet days; (b) Intensity: SDII – simple daily intensity index; (c) Frequency: R10mm – annual count of days when daily precipitation amount $\geq$ 10 mm; and d) Duration: CWD – annual maximum number of consecutive days with daily precipitation amount $\geq$ 1 mm, CDD – annual maximum number of consecutive days with daily precipitation amount < 1 mm from each of the 32 CMIP5 models. The extreme indices are recommended by the joint CCl/CLIVAR/JCOMM Expert Team (ET) on Climate Change Detection and Indices (ETCCDI).

A comprehensive assessment of each model's performance in each defined continent-climate zone group provides insight for users to select suitable models for their region of interest from a larger pool of models containing those with less skill. For instance, one can use the correlation and/or RMSE criteria in Fig. 50.7 to select a number of models among the 32 CMIP5 models for southeast China (CCZ6)

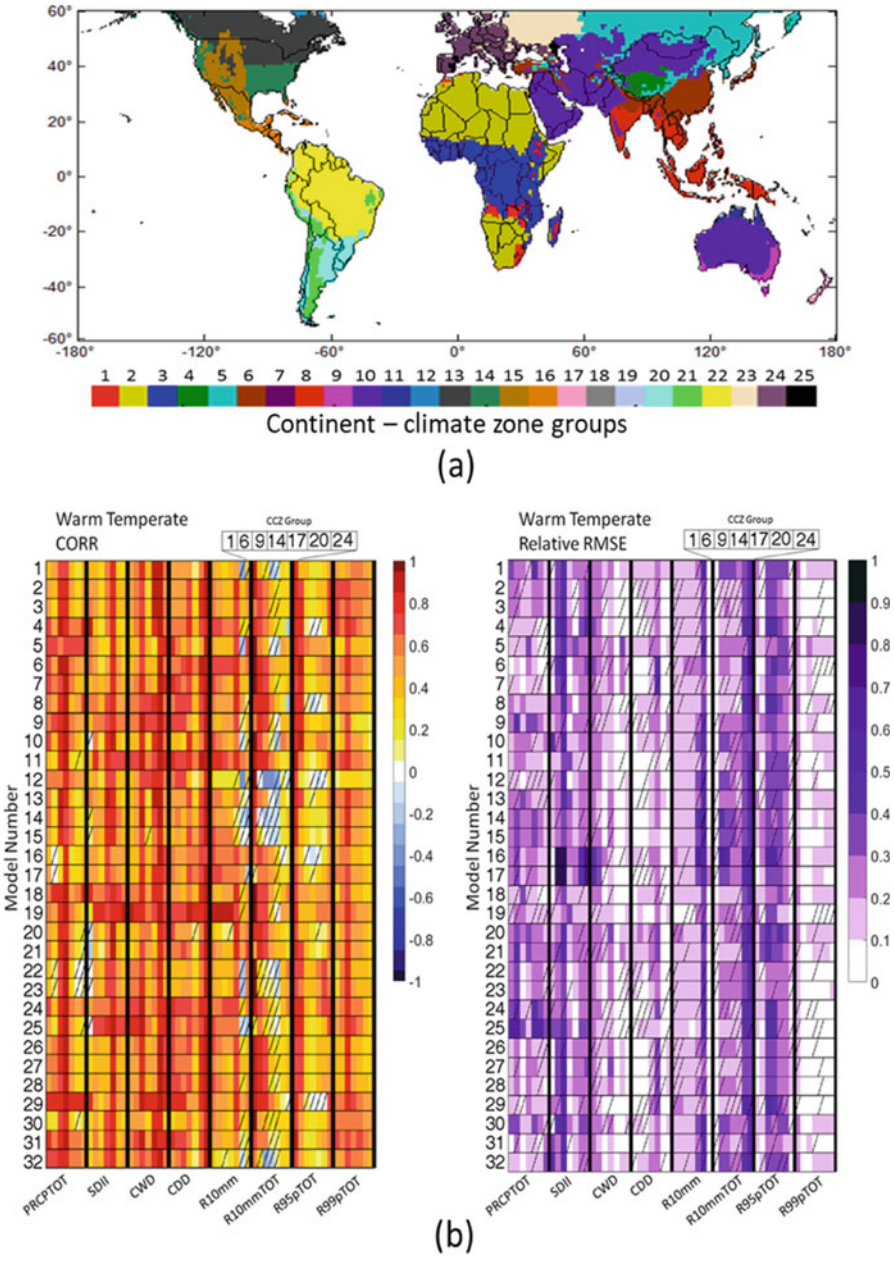

Fig. 50.7 (**a**) The 26 continent-climate zone groups, (**b**) Correlation (left) and relative RMSE (right) for precipitation indices in Warm Temperate continent-climate zone (CCZ) groups (statistical insignificance at 0.05 in hatched boxes). (Adapted from Nguyen et al. 2017b)

based on one or some of the 8 precipitation indices. If the selection is based on the simple daily intensity index (SDII) with the highest correlation, HadGEM2-ES, EC-EARTH, MIROC5 are the 3 best choices respectively. Such model selection can be adapted to any region globally depending on the phenomenon of interest, and can be combined with user-specific criteria.

50.3 Hydrology Applications

50.3.1 Hydrologic Modeling

Of more hydrological related applications of satellite-based precipitation products is rainfall-runoff modeling. With their continuous coverage both in space and time, satellite products bring invaluable information in modeling extreme events such as floods and droughts. In order to investigate the capability and accuracy of PERSIANN-CDR in modeling streamflow, PERSIANN-CDR's daily precipitation data are used in the NOAA's National Weather Service (NWS) Distributed Hydrologic Model Intercomparison Project – Phase 2 (DMIP2) test frame. Three test basins from Oklahoma are chosen. It is essential that as the very initial steps of conducting any study with satellite-products, the quality of satellite products be tested against ground-truth observations. The Taylor diagram in Fig. 50.8 illustrates

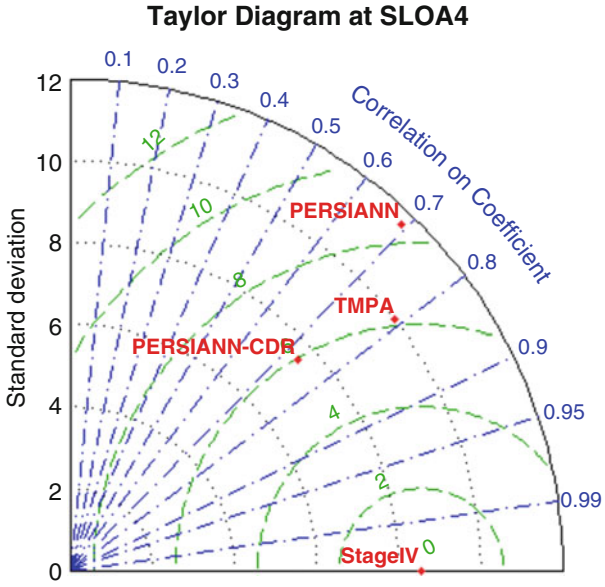

Fig. 50.8 Precipitation comparison plots SLOA4 basins between PERSIANN, PERSIANN-CDR, and TMPA against Stage IV gauge-adjusted radar data for 2003–2010. (Adapted from Ashouri et al. 2016a, b)

the evaluations of PERSIANN, PERSIANN-CDR, and TMPA precipitation products against Stage IV gauge-adjusted radar data as the reference dataset for SLOA4 basin. As shown PERSIANN-CDR and TMPA show close agreement with a relatively higher correlation coefficient (values on the arch) for TMPA, lower standard deviation (values on the y-axis) for PERSIANN-CDR, and almost the same root mean square deviation (RMSD; values on dashed curved lines) for both products.

With respect to the hydrological model, the widely used NOAA/NWS/Office of Hydrologic Development's HL-RDHM (Koren et al. 2003, 2004, 2014) was selected as the hydrological model to simulate the streamflow using the precipitation data products. Figure 50.9 illustrates the comparison between the observed and simulated streamflow from Stage IV, TMPA, PERSIANN, and PERSIANN-CDR over SLOA4 basin from 2003 to 2010. As can be seen, the performance of PERSIANN-CDR is satisfying when compared to Stage IV and TMPA products but PERSIANN-CDR has the capability to extend streamflow simulation back to 1983 where other high-resolution products are not available.

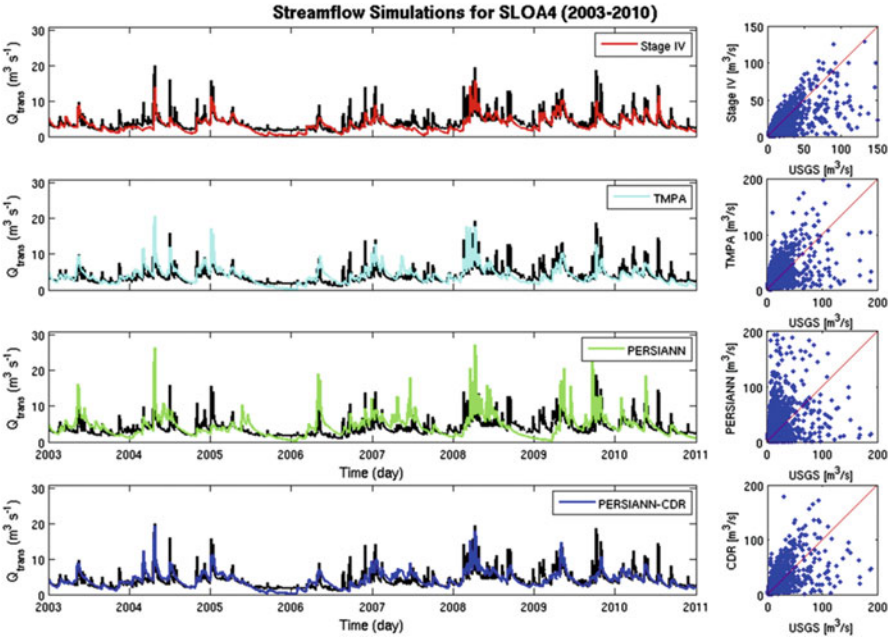

Fig. 50.9 Simulated and observed streamflow hydrographs and respective scatterplots at the outlet of SAVOY basin using (from top to bottom) Stage IV, TMPA, PERSIANN, and PERSIANN-CDR precipitation products. The solid black line shows the USGS observations. (Adapted from Ashouri et al. 2016a, b)

50.3.2 Rainfall Frequency Analysis Using Satellite-Retrieved Precipitation

In recent years, a handful of studies examined utilizing satellite-retrieved precipitation in rainfall frequency analysis to develop Intensity-Duration-Frequency (IDF) curves (e.g., Endreny and Imbeah 2009; Awadallah et al. 2011; Marra et al. 2017; Ombadi et al. 2018). This application of satellite-based precipitation datasets is of utmost importance to the developing countries where in-situ rainfall measurement has sparse distribution, insufficient record length and poor data quality. Furthermore, even in regions with dense ground-based rainfall gauge networks, satellite-based precipitation can provide valuable information about the spatial distribution of rainfall. This is primarily because precipitation retrieval algorithms from satellites provide area-averaged rainfall estimates unlike ground gauge observation which represent point measurements.

Among the satellite-based precipitation products that have been used for rainfall frequency analysis is PERSIANN-CDR. It represents a unique dataset due to its long historical record (1983 – present) which provides sufficient sample size for frequency analysis. Recently, the potential of using PERSIANN-CDR to develop IDF curves has been investigated (Ombadi et al. 2018; Gado et al. 2017). Ombadi et al. (2018) developed a general framework for developing IDF curves from satellite-retrieved precipitation. It is based mainly on two steps, firstly, bias adjustment using a regression model that utilizes elevation as a predictor variable, secondly, transformation of areal rainfall to point rainfall. The parameters of the bias adjustment model for PERSIANN-CDR were estimated over the Contiguous United States (CONUS) using CPC Unified Gauge-Based Analysis of Daily Precipitation over CONUS. The transformation of areal-to-point rainfall is necessary to develop point IDF curves since satellite-based precipitation products estimate an areal average of rainfall over a grid cell. Ombadi et al. (2018) adopted an approach for rainfall transformation that is used for the reverse transformation (i.e., point-to-area); the method is based on the stochastic representation of rainfall fields in space and time (Sivapalan and Blöschl 1998).

The framework was evaluated by developing IDF curves over CONUS and the results were compared to NOAA Atlas 14 (Bonnin et al. 2006, Perica et al. 2013). Figure 50.10 shows the distribution of relative errors of IDF curves developed from PERSIANN-CDR in comparison to NOAA Atlas 14. The results highlight the potential of using satellite-based precipitation datasets in developing IDF curves, median relative errors are in the range of (17–22%), (6–12%) and (3–8%) for 1-, 2- and 3-days IDFs, respectively, and return periods in the 2–100-year range.

Also, in a recent study (Gado et al. 2017), PERSIANN-CDR dataset has been used as an alternative approach to implement regional frequency analysis. Regional frequency analysis is commonly implemented in rainfall frequency analysis either to estimate design rainfalls at ungauged sites or to improve statistical inference by providing a larger sample size. Traditional regional frequency analysis is implemented by firstly delineating homogenous groups of sites. This step can be

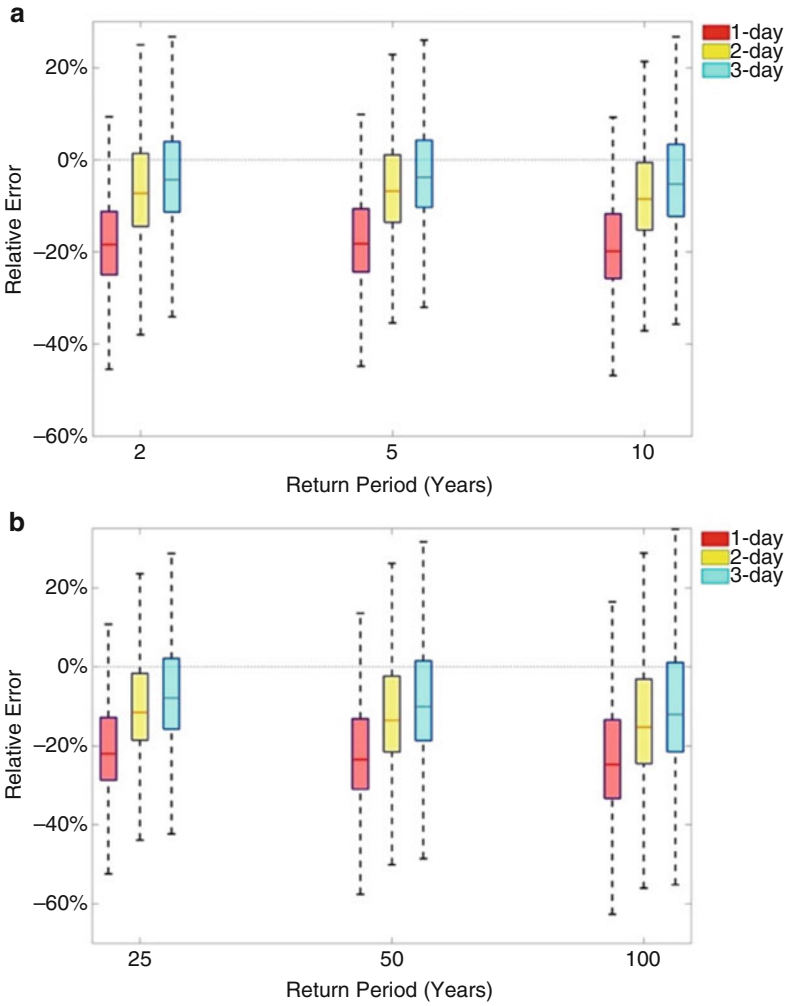

Fig. 50.10 Boxplots of satellite-based IDF relative error for durations of (1, 2 and 3) days and return periods of 25, 50 and 100 years. (Adapted from Ombadi et al. 2018)

performed using different methods such as cluster analysis (Tasker 1982), discriminant analysis (Wiltshire 1986), region of influence (Burn 1990) and the widely used method of discordancy measure (Hosking and Wallis 1993). The new approach is geared toward the estimation of design rainfalls at ungauged locations within a partially-gauged homogenous region and it consists of three steps. Firstly, satellite-based precipitation is adjusted for bias using the probability matching method (Calheiros and Zawadzki 1987). The distributions are constructed from satellite-based and in-situ rainfall measurements. Secondly, a relationship is constructed between original and corrected satellite-based precipitation. This

Table 50.1 Evaluation results of the two regional frequency approaches: Index Flood Method (IFM) and Regional Rainfall Frequency Analysis using Satellite Precipitation (RRFA-S)

RMSE (mm)			
Colorado		California	
IFM	RRFA-S	IFM	RRFA-S
4.09	5.95	6.13	5.05
7.05	8.45	7.77	6.09
13.42	13.38	10.33	7.88
20.36	18.73	12.67	9.78
29.49	25.85	15.43	12.29
41.28	35.15	18.68	15.53
82.44	68.33	28.51	26.24
37.86	19.32	15.88	13.63

Adapted from Gado et al. (2017)
Underlined values indicate the best result in each site

relationship is derived from gauged sites at a homogenous region and it is assumed to be valid for ungauged sites in the same region. Finally, this relationship is used to correct satellite-based precipitation at ungauged sites and derive IDF curves.

This method has been implemented to derive IDF curves over two regions in Colorado and California with 11 and 18 gauged sites respectively. These two regions have been identified as homogenous from previous studies (Sveinsson et al. 2002; Bonnin et al. 2011). In order to assess the performance of the methodology, the leave-one-out cross-validation was used to compare the accuracy of the methodology with the traditional index flood method. This is achieved by estimating the quantiles at a specific gauged site using the two approaches while neglecting data from that specific site. Then, the results are compared against at-site quantile estimates. The results in terms of the selected metrics, namely Bias, Relative Bias, Root Mean Square Error (RMSE) and relative RMSE indicated that the regional frequency analysis based on satellite-based precipitation provides more accurate results in most sites. In particular, it can be clearly seen that RMSE values, shown in Table 50.1, are considerably reduced using the approach based on satellite-retrieved precipitation.

50.4 Conclusions

There is a great zeal in current decades to investigate hydrologic and hydro-climatic processes with the availability and high reliability of ever-growing remotely sensed information. Characteristics such as high spatiotemporal resolution, real-time near-global coverage, make a wide range of applications viable through the incorporation of satellite-retrieved precipitation datasets such as PERSIANN-CDR.

Among the most important applications are the investigation of trends and changes of many hydroclimatic processes such as precipitation regimes response or the frequency and intensity of floods. Hurricane Katrina has been studied as an

example of extreme precipitation event to compare the rainfall patterns to the radar data and high-resolution satellite-based precipitation products from TMPA v7. The results show a higher correlation coefficient for PERSIANN-CDR than TMPA compared to Stage IV radar data, however, the bias in TMPA is lower than that in PERSIANN-CDR. In terms of count related indices PERSIANN-CCS in general produces the same patterns as CPC Unified Gauge-Based Analysis of Precipitation data. Another extreme precipitation study over China is conducted to assess the performance of PERSIANN-CDR in capturing extreme rainfall events, and was validated against gauge observation. PERSIANN-CDR captures the spatial distribution of the 99th (RR99p) and 95th (RR95p) percentile indices of the daily precipitation during the period of 1983–2006 similar to what the East Asia ground-based gridded daily precipitation data set shows.

Two case studies have been highlighted as examples of utilizing satellite-based precipitation datasets for hydrologic applications. Firstly, runoff prediction by forcing hydrologic models with satellite-based precipitation datasets. In the case study of Ashouri et al. (2016a, b), PERSIANN-CDR dataset has been used to predict runoff in three sub-basins of the Illinois River basin. The results demonstrated that PERSIANN-CDR-derived streamflow simulations are comparable to USGS observations in terms of correlation coefficients, bias, and index of agreement criterion. Secondly, the use of satellite-based precipitation in rainfall frequency analysis. In the study of Gado et al. (2017), a new approach to regional frequency analysis was proposed using PERSIANN-CDR dataset. The methodology was evaluated in two homogenous regions in Colorado and California; results demonstrated the efficiency of the methodology.

In the coming years, it is expected that satellite-based precipitation will play a fundamental role in hydrometeorological research. Given the continuous advancement in satellite sensors technology and retrieval algorithms, satellite-based precipitation datasets will be available in an improved spatiotemporal resolution. This is of utmost importance to the observation of precipitation heterogeneous nature, thus, enabling comprehensive investigation of key hydrometeorological processes. Moreover, as records of satellite-based precipitation extend to cover more years, trend analysis studies will be more conceivable. Similarly, extended record length will facilitate the utilization of satellite-based precipitation in rainfall frequency analysis for infrastructure design.

Acknowledgements This research was partially supported by the NASA Precipitation Measurement Missions (award # NNX10AK07G), NASA MEaSURES (award # NNX13AM12G), NASA MIRO (award # NNX15AQ06A), the ICIWaRM of the US Army corps of Engineering, UNESCO's G-WADI program, Cooperative Institute for Climate and Satellites (CICS) program (NOAA prime award #NA14NES4320003, subaward # 2014-2913-03) for OHD-NWS student fellowship, Army Research Office (award # W911NF-11-1-0422), National Science Foundation (NSF award # 1331915), Department of Energy (DoE prime award # DE-IA0000018) and California Energy Commission (CEC Award # 300-15-005).

References

Ashouri, H., Hsu, K.-L., Sorooshian, S., Braithwaite, D. K., Knapp, K. R., Cecil, L. D., Nelson, B. R., & Prat, O. P. (2015). PERSIANN-CDR: Daily precipitation climate data record from multisatellite observations for hydrological and climate studies. *Bulletin of the American Meteorological Society, 96*, 69–83. https://doi.org/10.1175/BAMS-D-13-00068.1.

Ashouri, H., Nguyen, P., Thorstensen, A., Hsu, K.-L., Sorooshian, S., & Braithwaite, D. (2016a). Assessing the efficacy of high-resolution satellite-based PERSIANN-CDR precipitation product in simulating streamflow. *Journal of Hydrometeorology, 17*, 2061–2076. https://doi.org/10.1175/JHM-D-15-0192.1.

Ashouri, H., Sorooshian, S., Hsu, K.-L., Bosilovich, M. G., Lee, J., Wehner, M. F., & Collow, A. (2016b). Evaluation of NASA's MERRA precipitation product in reproducing the observed trend and distribution of extreme precipitation events in the United States. *Journal of Hydrometeorology, 17*, 693–711. https://doi.org/10.1175/JHM-D-15-0097.1.

Awadallah, G. A., El Gamal, M., El Mostafa, A., & El Badry, H. (2011). Developing intensity-duration-frequency curves in scarce data region: An approach using regional analysis and satellite data. *Engineering, 3*, 215–226. https://doi.org/10.4236/eng.2011.33025.

Behrangi, A., Khakbaz, B., Jaw, T. C., AghaKouchak, A., Hsu, K.-L., & Sorooshian, S. (2011). Hydrologic evaluation of satellite precipitation products over a mid-size basin. *Journal of Hydrology, 397*, 225–237. https://doi.org/10.1016/j.jhydrol.2010.11.043.

Bonnin, G. M., Martin, D., Lin, B., Parzybok, T., Yekta, M., & Riley, D. (2006). NOAA Atlas 14 Volume 2 Version 3.0, Precipitation-Frequency Atlas of the United States. Silver Spring, MD, NOAA, National Weather Service, 295 pp. Available at http://www.nws.noaa.gov/oh/hdsc/PF_documents/Atlas14_Volume2.pdf, last accessed 24 Nov 2018.

Bonnin, G. M., Martin, D., Lin, B., Parzybok, T., Yekta, M., & Riley, D. (2011). NOAA Atlas 14 Volume 1 Version 5.0, Precipitation-Frequency Atlas of the United States. Silver Spring, MD, NOAA, National Weather Service. Available at http://www.nws.noaa.gov/oh/hdsc/PF_documents/Atlas14_Volume1.pdf, last accessed 24 Nov 2018.

Burn, D. H. (1990). Evaluation of regional flood frequency analysis with a region of influence approach. *Water Resources Research, 26*, 2257–2265. https://doi.org/10.1029/WR026i010p02257.

Calheiros, R. V., & Zawadzki, I. (1987). Reflectivity-rain rate relationships for radar hydrology in Brazil. *Journal of Climate and Applied Meteorology, 26*, 118–132. https://doi.org/10.1175/1520-0450(1987)026<0118:RRRRFR>2.0.CO;2.

Casse, C., & Gosset, M. (2015). Analysis of hydrological changes and flood increase in Niamey based on the PERSIANN-CDR satellite rainfall estimate and hydrological simulations over the 1983–2013 period. *Proceedings of the International Association of Hydrological Sciences, 370*, 117–123. https://doi.org/10.5194/piahs-370-117-2015.

Chiang, Y. M., Hsu, K.-L., Chang, F.-J., Hong, Y., & Sorooshian, S. (2007). Merging multiple precipitation sources for flood forecasting. *Journal of Hydrology, 340*, 183–196. https://doi.org/10.1016/j.jhydrol.2007.04.007.

Damberg, L., & AghaKouchak, A. (2014). Global trends and patterns of drought from space. *Theoretical and Applied Climatology, 117*, 441–448. https://doi.org/10.1007/s00704-013-1019-5.

Duan, Z., Liu, J., Tuo, Y., Chiogna, G., & Disse, M. (2016). Evaluation of eight high spatial resolution gridded precipitation products in Adige Basin (Italy) at multiple temporal and spatial scales. *Science of the Total Environment, 573*, 1536–1553. https://doi.org/10.1016/j.scitotenv.2016.08.213.

Endreny, T. A., & Imbeah, N. (2009). Generating robust rainfall intensity–duration–frequency estimates with short-record satellite data. *Journal of Hydrology, 371*, 182–191. https://doi.org/10.1016/j.jhydrol.2009.03.027.

Gado, T. A., Hsu, K.-L., & Sorooshian, S. (2017). Rainfall frequency analysis for ungauged sites using satellite precipitation products. *Journal of Hydrology, 554*, 646–655. https://doi.org/10.1016/j.jhydrol.2017.09.043.

Graumann, A., and National Climatic Data Center (US). (2006). Hurricane Katrina: A climatological perspective: preliminary report, Asheville, NC, U.S. Dept. of Commerce, National Oceanic and Atmospheric Administration, National Environmental Satellite Data and Information Service, National Climatic Data Center, 27 pp. Available at https://iucat.iu.edu/iue/8006266, last accessed 24 Nov 2018.

Hong, Y., Gochis, D., Cheng, J. T., Hsu, K.-L., & Sorooshian, S. (2007). Evaluation of PERSIANN-CCS rainfall measurement using the NAME event rain gauge network. *Journal of Hydrometeorology, 8*, 469–482. https://doi.org/10.1175/JHM574.1.

Hosking, J. R. M., & Wallis, J. R. (1993). Some statistics useful in regional frequency analysis. *Water Resources Research, 29*, 271–281. https://doi.org/10.1029/92WR01980.

Hsu, K.-L., Gao, X., Sorooshian, S., & Gupta, H. V. (1997). Precipitation estimation from remotely sensed information using artificial neural networks. *Journal of Applied Meteorology, 36*, 1176–1190. https://doi.org/10.1175/1520-0450(1997)036<1176:PEFRSI>2.0.CO;2.

Hsu, K.-L., Sellars, S., Nguyen, P., Braithwaite, D., & Chu, W. (2013). G-WADI PERSIANN-CCS GeoServer for extreme event analysis. *Sciences in Cold and Arid Regions, 5*, 6–15. https://doi.org/10.3724/SP.J.1226.2013.00006.

Huffman, G. J., Adler, R. F., Morrissey, M. M., Bolvin, D. T., Curtis, S., Joyce, R., McGavock, B., & Susskind, J. (2001). Global precipitation at one-degree daily resolution from multisatellite observations. *Journal of Hydrometeorology, 2*, 36–50. https://doi.org/10.1175/1525-7541(2001)0022.0.CO;2.

Huffman, G. J., Bolvin, D. T., Nelkin, E. J., Wolff, D. B., Adler, R. F., Gu, G., Hong, Y., Bowman, K. P., & Stocker, E. F. (2007). The TRMM multisatellite precipitation analysis (TMPA): Quasi-global, multiyear, combined-sensor precipitation estimates at fine scales. *Journal of Hydrometeorology, 8*, 38–55. https://doi.org/10.1175/JHM560.1.

Joyce, R. J., Janowiak, J. E., Arkin, P. A., & Xie, P. (2004). CMORPH: A method that produces global precipitation estimates from passive microwave and infrared data at high spatial and temporal resolution. *Journal of Hydrometeorology, 5*, 487–503. https://doi.org/10.1175/1525-7541(2004)005<0487:CAMTPG>2.0.CO;2.

Kendall, M. (1976). *Rank Correlation Methods* (4th ed.). London: Griffin.

Khanna, J., Medvigy, D., Fueglistaler, S., & Walko, R. (2017). Regional dry-season climate changes due to three decades of Amazonian deforestation. *Nature Climate Change, 7*, 200–204. https://doi.org/10.1038/nclimate3226.

Kidd, C., & Levizzani, V. (2011). Status of satellite precipitation retrievals. *Hydrology and Earth System Sciences, 15*, 1109–1116. https://doi.org/10.5194/hess-15-1109-2011.

Kidd, C., Becker, A., Huffman, G. J., Muller, C. L., Joe, P., Skofronick-Jackson, G., & Kirschbaum, D. B. (2017). So, how much of the Earth's surface is covered by rain gauges? *Bulletin of the American Meteorological Society, 98*, 69–78. https://doi.org/10.1175/BAMS-D-14-00283.1.

Klein Tank, A. M. G., Zwiers, F. W., & Zhang, X. (2009). Guidelines on analysis of extremes in a changing climate in support of informed decisions for adaptation, climate data and monitoring. WCDMP-No 72. WMO-TD No 1500, 56 pp. Available at https://www.ecad.eu/documents/WCDMP_72_TD_1500_en_1.pdf, last accessed 24 Nov 2018.

Koren, V., Smith, M., & Duan, Q. (2003). Use of a priori parameter estimates in the derivation of spatially consistent parameter sets of rainfall-runoff models. *Calibration of Watershed Models, 6*, 239–254. https://doi.org/10.1002/9781118665671.ch18.

Koren, V., Reed, S., Smith, M., Zhang, Z., & Seo, D. J. (2004). Hydrology laboratory research modeling system (HL-RMS) of the US national weather service. *Journal of Hydrology, 291*, 297–318. https://doi.org/10.1016/j.jhydrol.2003.12.039.

Koren, V. I., Smith, M. B., Cui, Z., & Cosgrove, B. A. (2014). Physically-based modifications to the Sacramento Soil Moisture Accounting model. Part A: Modeling the effects of frozen ground on the runoff generation process. *Journal of Hydrology, 519*, 3475–3491. https://doi.org/10.1016/j.jhydrol.2014.03.004.

Lee, H. T. (2014). Climate algorithm theoretical basis document (C-ATBD): Outgoing longwave radiation (OLR)—Daily. NOAA's Climate Data Record (CDR) Program. Tech. Rep. CDRP-ATBD-0526, 46 pp. Available at https://www1.ncdc.noaa.gov/pub/data/sds/cdr/CDRs/

Outgoing%20Longwave%20Radiation%20-%20Daily/AlgorithmDescription.pdf, last accessed 24 Nov 2018.

Lin, Y., & Mitchell, K. E. (2005). 1.2 the NCEP stage II/IV hourly precipitation analyses: Development and applications. 19th conference on Hydrology. Available at https://ams.confex.com/ams/Annual2005/techprogram/paper_83847.htm, last accessed 24Nov 2018.

Liu, X., Yang, T., Hsu, K.-L., & Sorooshian, S. (2017). Evaluating the streamflow simulation capability of PERSIANN-CDR daily rainfall products in two river basins on the Tibetan Plateau. *Hydrology and Earth System Sciences, 21*, 169–181. https://doi.org/10.5194/hess-21-169-2017.

Maggioni, V., Meyers, P. C., & Robinson, M. D. (2016). A review of merged high-resolution satellite precipitation product accuracy during the Tropical Rainfall Measuring Mission (TRMM) era. *Journal of Hydrometeorology, 17*, 1101–1117. https://doi.org/10.1175/JHM-D-15-0190.1.

Mann, H. B. (1945). Nonparametric tests against trend. Econometrica: Journal of Econometric Society, 245–259. Available qat https://www.jstor.org/stable/1907187?seq=1#metadata_info_tab_contents, last accessed 24 Nov 2018.

Marra, F., Morin, E., Peleg, N., Mei, Y., & Anagnostou, E. N. (2017). Intensity–duration–frequency curves from remote sensing rainfall estimates: Comparing satellite and weather radar over the eastern Mediterranean. *Hydrology and Earth System Sciences, 21*, 2389–2404. https://doi.org/10.5194/hess-21-2389-2017.

Miao, C., Ashouri, H., Hsu, K., Sorooshian, S., & Duan, Q. (2015). Evaluation of the PERSIANN-CDR Daily Rainfall Estimates in Capturing the Behavior of Extreme Precipitation Events over China. *Journal of Hydrometeorology, 16*, 1387–1396. https://doi.org/10.1175/JHM-D-14-0174.1.

Nguyen, P., Sellars, S., Thorstensen, A., Tao, Y., Ashouri, H., Braithwaite, D., Hsu, K., & Sorooshian, S. (2014). Satellites track precipitation of Super Typhoon Haiyan. *EOS Transactions, 95*, 133–135. https://doi.org/10.1002/2014EO160002.

Nguyen, P., Sorooshian, S., Thorstensen, A., Tran, H., Huynh, P., Pham, T., Ashouri, H., Hsu, K.-L., AghaKouchak, A., & Braithwaite, D. (2017a). Exploring trends through "RainSphere": Research data transformed into public knowledge. *Bulletin of the American Meteorological Society, 98*, 653–658. https://doi.org/10.1175/BAMS-D-16-0036.1.

Nguyen, P., Thorstensen, A., Sorooshian, S., Zhu, Q., Tran, H., Ashouri, H., Miao, C., Hsu, K.-L., & Gao, X. (2017b). Evaluation of CMIP5 model precipitation using PERSIANN-CDR. *Journal of Hydrometeorology, 18*, 2313–2330. https://doi.org/10.1175/JHM-D-16-0201.1.

Nguyen, P., Thorstensen, A., Sorooshian, S., Hsu, K.-L., AghaKouchak, A., Ashouri, H., Tran, H., & Braithwaite, D. (2018). Global precipitation trends across spatial scales using satellite observations. *Bulletin of the American Meteorological Society, 99*, 689–697. https://doi.org/10.1175/BAMS-D-17-0065.1.

Ombadi, M., Nguyen, P., Sorooshian, S., & Hsu, K. (2018). Developing intensity-duration-frequency (IDF) curves from satellite-based precipitation: Methodology and evaluation. *Water Resources Research, 54*, 7752–7766. https://doi.org/10.1029/2018WR022929.

Perica, S., Martin, D., Pavlovic, S., Roy, I., Laurent, M. S., Trypaluk, C., et al. (2013). NOAA Atlas 14, Volume 9, Version 2, Precipitation-Frequency Atlas of the United States, Southeastern States (Vol. 18). Silver Spring, MD: NOAA, National Weather Service.

Rana, S., McGregor, J., & Renwick, J. (2015). Precipitation seasonality over the Indian subcontinent: An evaluation of gauge, reanalyses, and satellite retrievals. *Journal of Hydrometeorology, 16*, 631–651. https://doi.org/10.1175/JHM-D-14-0106.1.

Sivapalan, M., & Blöschl, G. (1998). Transformation of point rainfall to areal rainfall: Intensity-duration-frequency curves. *Journal of Hydrology, 204*, 150–167. https://doi.org/10.1016/S0022-1694(97)00117-0.

Sorooshian, S., Hsu, K.-L., Gao, X., Gupta, H. V., Imam, B., & Braithwaite, D. (2000). Evaluation of PERSIANN system satellite–based estimates of tropical rainfall. *Bulletin of the American Meteorological Society, 81*, 2035–2046. https://doi.org/10.1175/1520-0477(2000)081<2035:EOPSSE>2.3.CO;2.

Sorooshian, S., Gao, X., Hsu, K.-L., Maddox, R. A., Hong, Y., Gupta, H. V., & Imam, B. (2002). Diurnal variability of tropical rainfall retrieved from combined GOES and TRMM satellite information. *Journal of Climate, 15*, 983–1001. https://doi.org/10.1175/1520-0442(2002)015<0983:DVOTRR>2.0.CO;2.

Sorooshian, S., AghaKouchak, A., Arkin, P., Eylander, J., Foufoula-Georgiou, E., Harmon, R., Hendrickx, J. M., Imam, B., Kuligowski, R., Skahill, B., & Skofronick-Jackson, G. (2011). Advancing the remote sensing of precipitation. *Bulletin of the American Meteorological Society, 92*, 1271–1272. https://doi.org/10.1175/BAMS-D-11-00116.1.

Sun, Q., Miao, C., Duan, Q., Ashouri, H., Sorooshian, S., & Hsu, K.-L. (2018). A review of global precipitation data sets: Data sources, estimation, and intercomparisons. *Reviews of Geophysics, 56*, 79–107. https://doi.org/10.1002/2017RG000574.

Sveinsson, O. G., Salas, J. D., & Boes, D. C. (2002). Regional frequency analysis of extreme precipitation in northeastern Colorado and Fort Collins flood of 1997. *Journal of Hydrologic Engineering, 7*, 49–63. https://doi.org/10.1061/(ASCE)1084-0699(2002)7:1(49).

Tan, M. L., Ibrahim, A. L., Duan, Z., Cracknell, A. P., & Chaplot, V. (2015). Evaluation of Six High-Resolution Satellite and Ground-Based Precipitation Products over Malaysia. *Remote Sensing, 7*, 1504–1528. https://doi.org/10.3390/rs70201504.

Tasker, G. D. (1982). Comparing methods of hydrologic regionalization. *Journal of the American Water Resources Association, 18*, 965–970. https://doi.org/10.1111/j.1752-1688.1982.tb00102.x.

Taylor, K. E., Stouffer, R. J., & Meehl, G. A. (2012). An overview of CMIP5 and the experiment design. *Bulletin of the American Meteorological Society, 93*, 485–498. https://doi.org/10.1175/BAMS-D-11-00094.1.

Wiltshire, S. E. (1986). Regional flood frequency analysis I: Homogeneity statistics. *Hydrological Sciences Journal, 31*, 321–333. https://doi.org/10.1080/02626668609491051.

Xie, P., & Arkin, P. A. (1997). Global precipitation: A 17-year monthly analysis based on gauge observations, satellite estimates, and numerical model outputs. *Bulletin of the American Meteorological Society, 78*, 2539–2558. https://doi.org/10.1175/1520-0477(1997)078<2539:GPAYMA>2.0.CO;2.

Xie, P., Janowiak, J. E., Arkin, P. A., Adler, R. F., Gruber, A., Ferraro, R. R., Huffman, G. J., & Curtis, S. (2003). GPCP pentad precipitation analyses: An experimental dataset based on gauge observations and satellite estimates. *Journal of Climate, 16*, 2197–2214. https://doi.org/10.1175/2769.1.

Xie, P., Chen, M., Yang, S., Yatagai, A., Hayasaka, T., Fukushima, Y., & Liu, C. (2007). A gauge-based analysis of daily precipitation over East Asia. *Journal of Hydrometeorology, 8*, 607–626. https://doi.org/10.1175/JHM583.1.

Xie, P., Chen, M., & Shi, W. (2010). CPC unified gauge-based analysis of global daily precipitation. Preprints, 24th Conference on Hydrology, Atlanta, GA, American Meteorological Society. (Vol. 2). Available at https://ams.confex.com/ams/90annual/techprogram/paper_163676.htm, last accessed 24 Nov 2018.

Yang, X., Yong, B., Yong, H., Chen, S., & Zhang, X. (2016). Error analysis of multi-satellite precipitation estimates with an independent raingauge observation network over a medium-sized humid basin. *Hydrological Sciences Journal, 61*, 1813–1830. https://doi.org/10.1080/02626667.2015.1040020.

Zambrano, F., Wardlow, B., Tadesse, T., Lillo-Saavedra, M., & Lagos, O. (2017). Evaluating satellite-derived long-term historical precipitation datasets for drought monitoring in Chile. *Atmospheric Research, 186*, 26–42. https://doi.org/10.1016/j.atmosres.2016.11.006.

Zhu, Q., Xuan, W., Liu, L., & Xu, Y. P. (2016). Evaluation and hydrological application of precipitation estimates derived from PERSIANN-CDR, TRMM 3B42V7, and NCEP-CFSR over humid regions in China. *Hydrocarbon Processing, 30*, 3061–3083. https://doi.org/10.1002/hyp.10846.